Pressure effects on interfacial surface contacts and performance of organic solar cells

Agyei-Tuffour, B.; Doumon, Nutifafa Y.; Rwenyagila, E. R. ; Asare, J. ; Oyewole, O. K. ; Shen, Z. ; Petoukhoff, C. E. ; Zebaze Kana, M. G. ; Ocarroll, D. M. ; Soboyejo, W. O.

Published in:
Journal of Applied Physics

DOI:
10.1063/1.5001765

Publication date:
2017

This manuscript was accepted by J. Appl. Phys. Click here to see the version of record.

Pressure Effects on Interfacial Surface Contacts and Performance of Organic Solar Cells

B. Agyei-Tuffour,[1,2,3] N.Y. Doumon,[4,5] E. R. Rwenyagila,[1] J. Asare,[4] O. K. Oyewole,[4] Z. Shen,[3] C. E. Petoukhoff,[3] M. G. Zebaze Kana,[4,6,8] D. M. Ocarroll,[3] and W. O. Soboyejo.[1,7,8,9]

[1]*Department of Materials Science and Engineering, African University of Science and Technology, Km 10, Airport Road, Abuja, Federal Capital Territory, Nigeria.*

[2]*Department of Materials Science and Engineering, School of Engineering Sciences, University of Ghana, Legon-Accra, Ghana.*

[3]*Institute of Advanced Materials, Devices and Nanotechnology, Department of Materials Science and Engineering, Rutgers University, Piscataway, New Jersey, USA.*

[4]*Department of Theoretical and Applied Physics, African University of Science and Technology, Km 10, Airport Road, Abuja, Federal Capital Territory, Nigeria.*

[5]*Zernike Institute for Advanced Materials, University of Groningen, Nijenborgh 4, NL-9747 AG, Groningen-The Netherlands*

[6]*Department of Materials Science and Engineering, Kwara State University, Ilorin, Kwara State, Nigeria.*

[7]*Department of Mechanical and Aerospace Engineering, Princeton Institute of Science and Technology of Materials (PRISM), Olden Street, Princeton, New Jersey, USA.*

[8]*Department of Mechanical Engineering, Materials Science and Engineering Program, Worcester Polytechnic Institute (WPI), 100 Institute Road, Worcester, MA 01609, USA.*

[9]*Department of Biomedical Engineering, Worcester Polytechnic Institute (WPI), Gateway Park Life Sciences and Bioengineering Center, 60 Prescott Street, Worcester, MA 01609, USA.*

Correspondence address:

Prof. Wole Soboyejo

Department of Mechanical and Aerospace Engineering, Princeton Institute of Science and Technology of Materials(PRISM), Olden Street, Princeton, New Jersey, USA.

This manuscript was accepted by J. Appl. Phys. Click here to see the version of record.

Email: soboyejo@aol.com, wsoboyejo@wpi.edu , Tel: +1 609 306 9614

Abstract

This paper explores the effects of pressure on the interfacial surface contacts and performance of organic solar cells. A combination of experimental techniques and analytical/computational models is used to study the evolving surface contacts profiles that occur when compliant, semi-rigid and rigid particles are interlocked between adjacent layers in model solar cell structures. The effects of layer surface roughness and interlocked (trapped) particles are also considered along with the effects of surface energy, adhesion energy and pressure. The results show that, increased interfacial contact lengths and decreased void lengths are associated with the application of increased pressure. Increased pressure also results in significant improvements in power conversion efficiency. These improvements in power conversion efficiency are associated with the closure up of micro- and nano-voids due to the application of pressure to layers produced via spin coating and thermal evaporation. The results suggest that pressure-induced contacts can be used to enhance the performance of organic solar cells.

Keywords: *Interfacial surface contacts, compliant and rigid thin films, solar cell performance*.

I. INTRODUCTION

Bulk heterojunction Organic Photovoltaics (OPVs) have attracted significant interest for large-area solar energy conversion.[1] This is due to their attractive combinations of efficiency (~5-10%) and fabricability from relatively cheap organic materials.[2] A typical OPV structure consists of: an inorganic Indium-tin oxide (ITO/Glass) anode; a poly(3,4-ethylenedioxythiophene:poly(styrenesulphonate)) (PEDOT:PSS) hole transport layer (HTL), and

This manuscript was accepted by J. Appl. Phys. Click here to see the version of record.

a poly(3-hexylthiophene):phenyl-C61 butyric acid methyl ester (P3HT:PCBM) bulk heterojunction photoactive layer. The electron transport layer (ETL), lithium fluoride (LiF), and a back contact cathode of aluminum complete the device. These HTL and ETL layers facilitate the separation of excitons into electrons and holes and conduct them to the respective electrodes. This gives high organic photovoltaic device performance.[2-4]

Prior work[5-7] has explored a range of HTL materials for Organic Photovoltaics (OPVs) and Organic Light Emitting Devices (OLEDs). These include studies by: Du *et al*.,[5] Tong *et al*.,[6] and Agyei-Tuffour *et al*.[7] These studies have shown that the performance of different HTL materials can have significant effects on the performance of OLEDs and OPVs. Inorganic HTLs: (vanadium pentoxide (V_2O_5), nickel oxide (NiO), tungsten trioxide (W_2O_3) and molybdenum trioxide (MoO_3)) have also been shown to enhance the power conversion efficiencies of OLEDs,[8-10] while the application of pressure has been shown to enhance the surface contacts between layers in OLEDs and OPVs. However, the application of excessive pressure can also lead to the sink-in of particles that exist between adjacent layers in OPVs and OLEDs. There is, therefore, a need to develop pressure-assisted methods for the fabrication of OLEDs and OPVs with minimal sink-in and improved surface contact that can promote charge and light transport between the layers.

Hence, in this paper, we present the results of a combined experimental and computational/analytical study of the effects of pressure on interfacial surface contacts between layers that are present in typical bulk heterojunction OPVs with PEDOT:PSS HTL. The effects of the applied pressure are studied in model bi-layers and OPV structures. Pressure is applied to the model bi-layers and OPV structures using poly dimethyl siloxane (PDMS) stamps. The effects of the film Young's moduli, adhesion energy and pressure (on interfacial contacts and

rigid lengths) are modeled using numerical and analytical simulations.[6] The results show that the interfacial surface contacts and OPV energy conversion efficiency improve with applied pressure. The results and their implications are discussed for the design of pressure-assisted fabrication processes.[11-16]

II. THEORY

A. Modeling of Surface Contacts

Organic thin films subjected to loading (pressure) may exhibit elastic and/or plastic deformation, depending on the nature of the film. The mechanical properties of the films and the trapped particles may influence the deformation. For instance, the Young's moduli of the films and the trapped particles may lead to the classification of the materials into rigid, semi-rigid and compliant materials. These different types of trapped particles can greatly influence the deformation behavior of adjacent films.

In the case of compliant organic thin films with trapped particles (silicone, PDMS, photoresist and textile polymer),[6] the deformation of the layers surrounding rigid trapped particles can be idealized by the deformation of cantilever beams. The resulting cantilever beam deflections, and the interfacial surface contacts between the adjacent layers, can therefore provide insights into the evolution of surface contact between adjacent layers in OPV structures.

When the trapped particles between the layers are rigid (ITO, MoO_3, silicon, aluminum, Iron, quartz), interfacial contact improvements can be difficult to achieve. Furthermore, trapped particles can sink-in into semi-rigid or compliant adjacent layers. The trapped particle sizes usually vary from ~ 0.1 μm to ~ 20 μm in diameter.[17,18] Prior work has shown that, increasing

pressure results in increased surface contact, while the void length lengths (S) decreases with increasing pressure. These can result in the increased performance of OPVs[16] and OLEDs.[5,15]

Prior analytical models[18-22] have been used to study the surface contacts around interlocked particles during the application of pressure. Figure 1 shows the application of pressure on bilayer and complete device models with varying surface morphologies. Figure 1(a) shows films of increased surface roughness and blister or trapped particle height prior to pressure application with the help of PDMS stamps. Figure 1(b) presents the films with relatively smooth surface morphologies before the application of pressure. In Figure 1(c) is the stacking of OPV layers into a complete device before the application of pressure. For a PEDOT:PSS film that forms a blister of radius, "r", upon sandwiching around a trapped particle (Figure 1), Du *et al.*,[5] Malyshev-Salganik *et al.*[21] and Wan-Mai *et al.*[22] have idealized the contact with a penny crack in bending. Hence, by considering the relationships between the surface energies, as well as the stored energies and other variables, they were able to determine the adhesion energy (γ) between the layers. This is given by:

$$\gamma = \frac{2Ew^3h^2}{3\left(1-\nu^2\right)r^4}, \tag{1}$$

where E is the Young's modulus and ν is the Poisson's ratio of the materials that form the organic solar cells; w and h, are respective thicknesses and heights of the trapped particles or blisters. When the film's width compared with the height of the trapped particle is adequately small, then, the film will undergo stretching and bending. Hence, the total energy stored in the film (U_T) is given by Du *et al.*[5] as:

This manuscript was accepted by J. Appl. Phys. Click here to see the version of record.

$$U_T = \frac{6EIh^2}{s^3} - \gamma w\left(L - s\right), \tag{2}$$

where I is the second moment of area and s is the length of void created. Previous work by Agyei-Tuffour *et al.*[7] has also shown that the void length (s) and contact length ratio (L_c/L) are related through the following expressions:

$$s = \left(\frac{3Ew^3h^2}{2\gamma}\right)^{\frac{1}{4}} \tag{3}$$

and

$$\frac{L_c}{L} = 1 - \frac{1}{L}\left(\frac{3}{2}\frac{Ew^3h^2}{\gamma}\right)^{1/4} \tag{4}$$

Similarly, the contact length can also be written as a function of the applied pressure according to Du *et al.*[5] and Asare *et al.*[28] These give:

$$\frac{L_c}{L} = 1 - \left[\frac{3\left(\frac{E}{\left(1-\nu^2\right)}\right)w^3h}{2PL^4}\right]^{\frac{1}{4}} \tag{5}$$

Since the properties of the thin layer materials are known,[6] the contact length and the void lengths can be accurately predicted from Equations 3 and 5. The adhesion energies can also be estimated for the different interfaces that are present in organic electronic structures.[5,6,7] Hence, using published data from the work of Du *et al.*[5] and Tong *et al.*,[6] the above analytical models can be used to estimate the contact length ratios between adjacent layers that are present in OPVs

and OLEDs. Similar results have also been reported for the cold-welded metallic thin films.[15,24,28]

B. Finite Element Modeling of Contacts

Finite element modeling was carried out using the ABAQUS CAE 6.12 software package (ABAQUS™, Simulia, Pawtucket, RI, USA). This was used to model interfacial contacts and void length profiles around the interlocked particles (blisters). The simulations considered the contacts profiles associated with a typical blister height of ~ 1 μm, which is representative of migrating airborne dust particles in clean room environments.[14] Similar assumptions have been made in prior work by Du *et al.*[5] and Moreau *et al.*[17]

The influence of surface morphology (surface roughness) was also considered in modeling the pressure effects with four node finite element mesh. Fine mesh were used in the simulation of contacts that had large displacements and relatively high stress gradients. The possibility of displacement and rotation about the bottom part of the substrate was eliminated by fixing the substrate. Lateral movements were also eliminated because the outer edge of the model was also fixed, as reported in prior work.[5, 7, 28] Assuming that all the thin films were isotropic, a uniform pressure of ~ 10 MPa[29] was applied to the stamp in the simulations. The deformation was then simulated (in ABAQUS) around trapped in the model OPV structures.

III. EXPERIMENTAL PROCEDURES

A. Photovoltaic Device Fabrication and Characterization

In order to validate the numerical and analytical models, pressure-assisted experiments were performed on model OPV devices and bi-layers. The model photovoltaic devices were fabricated from layers with a Glass/ITO/PEDOT:PSS/P3HT:$PC_{60}BM$/LiF/Al architecture. The effects of

This manuscript was accepted by J. Appl. Phys. Click here to see the version of record.

pressure (on the efficiencies of the devices) were studied by measuring the current-voltage characteristics of the OPVs with Keithley Model 2400 system (Keithley Instruments Inc., Cleveland, Ohio, USA). The surface/interfacial morphologies associated with the pressured films were observed in a Field Emission Gun Scanning Electron Microscope (FEGSEM, Carl-Zeiss Evo MA-10 SEM, Oberkochen, Germany) that was operated at a voltage of 10 –15 kV and a pressure of $4x10^{-6}$ mbar. Exposure of electrons was limited to 30 s to minimize the structural changes due to electron/material interactions. Grazing Incidence Wide Angle X-ray Scattering (GIWAXS) experiments were conducted on the polymer blend films to investigate the influence of pressure on polymer chain alignment, crystallinity and interfacial contact morphology. The experiments were carried out using a 13.5 keV and 9.18 nm wavelength x-ray beam at the X9 beamline, (NSLS, Brookhaven National Laboratory, USA) with grazing incidence angles ranging from ~0.07° to ~ 0.15°. The results presented in this paper are from incidence angle of ~0.12° which is above the critical angle of the polymer blend. 2D images and 1D line scans were collected and converted into q-space using silver behenate powder as the standard.

Devices were fabricated using patterned indium tin oxide (ITO) on glass substrates. The patterned ITO substrate was ultrasonically cleaned with acetone, ethanol and deionized water in succession. The substrates were then further cleaned in an Ultra-Violet Ozone system (UVOCS, Lansdale, PA, USA) for 10 minutes, before spin coating an ~ 40 nm thick layer of PEDOT:PSS into the ITO layer at 3500 rpm for 1 minute. The resulting composite was heat treated in air at 120°C for 10 minutes. This was followed by the deposition of the P3HT:PCBM active layer (20 mg/ml concentration of P3HT:PCBM in chlorobenzene was deposited at 700 rpm spin speed for 180 s to obtain ~ 80 nm thick films). The three-layered composite OPV system was transferred into an argon filled glove box and annealed at 140°C for 4 minutes. Subsequently, ~ 0.2 nm

protective layer of LiF and a 150 nm Al back contact layer were thermally deposited onto the three-layered structure to produce devices with cross-sectional surface areas of ~ 0.105 cm^2.

The current-voltage (I-V) characteristics of the resulting devices were measured before and after the application of pressure to PDMS stamps (diameter (ϕ) = 30 mm, thickness (δ) = 5 mm). Furthermore, since previous studies[5,29] have shown that pressures greater than ~10 MPa results in excessive particle sink-in that can cause layer damage and reduced photoconversion efficiency. An applied pressure of ~10 MPa was used in this study to explore the effects of applied pressure. This was also carried out at room-temperature (~ 25°C) under ambient conditions, as reported in prior work.[5,7,29]

IV. RESULTS AND DISCUSSION

A. Surface Characterization and interface morphology of Thin Films

Figure 2(a)-(e) presents typical SEM images of the interfacial surface morphologies of the layers in the P3HT:PCBM OPV structures. The SEM and optical micrographs as a function of pressure application are also shown. It can be observed that, increase in pressure leads to increase in relative smoothness in the surface morphology. The inserts in Figure 2 (i-vi) show the optical images showing the changes in the surface morphologies from the roughest to the smoothest films in the micro-scale. These surface changes confirm the observation from the AFM studies[29] that, the higher the applied pressure, the relatively smoother the films. The average surface roughness (R_a) values are presented in Table 1. These show that the PEDOT:PSS layer had R_a ~ 0.8±0.1 nm, while the P3HT:PCBM layer had R_a ~ 0.7±0.1 nm. Again from Table 1, the adhesion energies between the glass substrate, PEDOT:PSS and P3HT:PCBM are 9.3, 2.9 and 0.5 J/m^2, respectively. [6,31]

This manuscript was accepted by J. Appl. Phys. Click here to see the version of record.

The SEM micrographs establish the relationship between the interfacial contact morphologies and the applied pressure. It can be seen that the surface appearance shows relative decrease in surface roughness ranging from the pressure-less condition to the 15 MPa. The 10 MPa applied pressure produced the least roughness (~0.7+0.1) for P3HT:PCBM and (~0.8+0.1) for the PEDOT:PSS film. The enhancement in the surface smoothness improves the interfacial contacts and the transport of electrons and holes. These will also reduce the partial contacts and layer sink-in phenomena and hence the improvement in the device performance after pressure application.[7,29]

The pressure application on the OPV layers again lead to changes in the orientation of the polymer backbone chains in the P3HT and PEDOT:PSS. The bonds between the chain become stretched, elongated and orderly as presented in the GIWAXS out-of-plane and in-plane profiles in Figure 3(a-c). The schematic representation in Figure 3(a) shows the interaction between grazing incidence x-ray beam and the polymer blend film that have been subjected to ~ 10 MPa pressure. Figure 3(b) and Figure 3(c) present the 1D profile for the out-of-plane and the in-plane directions for P3HT and P3HT:PCBM films respectively. The (100), (200) and (300) peaks positions are associated with the out-of-plane and the dominant peak in the in-plane was the (010). Prior work[29,31-35] has shown that P3HT chains preferentially align themselves in the edge-on configuration with the π-π stacking in (010) direction. Therefore, with the application of pressure in the out-of-plane direction and perpendicular to the substrate, the bonds between the polymer backbones are also elongated in the in-plane direction leading to the edge-on configuration. This orientation of the polymer chain increases the OPV performance due to the enhancements in the polymer crystallinity in the blend.

Figure 4 presents the photo-absorbance enhancements in the active P3HT:PCBM layer after the application of pressure. The region of absorption of the P3HT:PCBM film also covers the ultra violet (UV) and visible ranges of the electromagnetic spectrum.

It is important to note here that, there is an active interaction between the P3HT and the PCBM in the active layer. In the samples without applied pressure, the absorbance in the polymer blend was observed to be marginal. However, this was not the case in the pressure applied samples because the absorbance of the P3HT:PCBM blend increased (Figures 4). This increase is attributed to the reduction in the surface roughness and increased polymer crystallinity, after the application of pressure to the films.[7,29,32]

B. Analytical Modeling of Adhesion and Contacts

The analytical predictions of the effects of pressure on contact lengths (obtained from Equations 1-5), are presented in Figures 5(a) – 5(b). These show that the contact length ratios increase, while the void lengths decrease with increasing applied pressure. The contact length also increases with increasing adhesion energy. This confirms that contact between the adjacent layers in OPVs can be controlled by the selection of adjacent materials with increased adhesion energy, and also by the application of pressure to the film stacks.

The above results show trends that are consistent with the results from previous studies[5,6,7] in which increasing applied pressure (on OLED layers) have been shown to reduce nano-void sizes, increase interfacial contacts and result in enhanced current-voltage characteristics of organic light emitting devices (OLEDs)[5] and in bulk heterojunction photovoltaic cells (OPVs).[6,7] The current results, therefore, suggest that enhanced interfacial contacts can be used to improve the performance of OPV devices.

This manuscript was accepted by J. Appl. Phys. Click here to see the version of record.

C. Finite Element Modeling of Layered OPV Structures

Figure 6 presents a finite element model of contact profiles in a layered OPV device subjected to applied pressure. The geometry of the evolved contacts and the formation of blisters, prior to the pressure application with the assistance of PDMS stamps, are also shown. The associated stress distributions in the layered structure and in the trapped particles are also presented in Figure 7. In Figure 7(a), the upper film shows no bending around the rigid trapped particle and the stresses are mainly concentrated around the trapped particle region. Figure 7(b) shows bending of the upper layer and trapped particle sink-in in the adjacent layers due to excessive pressure application. The stresses in the trapped particle are high compared to the stresses in the entire region of the OPV layers.

The high stresses around the trapped particle decrease with increasing distance from the particle. The von Mises stress distributions in the semi-rigid and compliant particles are lower than those around rigid particles in which the Mises stresses are much higher around the trapped particles. These clearly show that the Young's moduli of the trapped particles strongly affect the stress concentrations around the trapped particles. Such high stresses can in turn lead to the degradation of the multilayered structures of the OPVs.

High modulus particles such as aluminum (~70 GPa), MoO_3 (~64.6 GPa), plain carbon steel (~205 GPa), in Table 1, result in high stress concentrations that can lead to device degradation and failure of OPV structures. Intermediate and lower modulus particles such as poly-2-methoxy-5-(2- ethylhexyloxy)-1,4-phenylenevinylene (MEH:PPV (~ 11.5 GPa)), PEDOT:PSS (~1.56 GPa), P3HT:PCBM (~ 6.02 GPa), etc., easily deform to improve the contact length ratios. They also distribute the stresses within the entire region of contact.

Typical deformation profiles around the trapped particles are shown in Figure 8. The smooth surface morphologies and soft trapped particles require lower pressures to achieve enhanced contact length, while rougher surface morphologies and rigid trapped particles require higher pressures to achieve improved contact lengths. In most cases, the latter results in multiple partial contacts and particle sink-in, this degrades the device performance. Hence, pressure-assisted fabrication of OPVs should not use applied pressures above ~10 MPa. This result agrees with studies by Du *et al.*[5] Akande *et al.,*[24] and Agyei-Tuffour *et al.*[7,29] who reported ~ 8.6 MPa for pressure-assisted OLED fabrication, and ~ 10 MPa pressure for OPV fabrication.

D. Performance of OPVs

The performance of OPVs was characterized using the energy conversion efficiencies associated with the measured current-voltage characteristics. This was done before and after the application of pressure (~ 10 MPa). The results of the current density-voltage measurements are presented in Figure 9 for the OPV, before and after the application of pressure. After pressure application, ~ 18% increase in the short circuit current (I_{sc}) was observed, with a corresponding 7.20% increase in the fill factor. The efficiency of the OPV also increased from ~3.5% to ~ 4.4%, following the application of pressure. This represents an average increase of ~25% in the efficiency of the OPV device. It is important to note, however, that the devices with PEDOT:PSS and P3HT:PCBM layers experienced significantly increased contacts. Hence, the observed increase in the photo-conversion efficiencies is associated with the improved interfacial contacts that can occur in these layers, following the application of pressure to the film stacks. It is postulated that these can enhance the transport of light and charge across the interfaces.

E. Implications

The implications of the results are very significant. Firstly, the study shows that, the power conversion efficiencies of OPVs can be significantly improved by the application of pressure. This causes voids to close up, thereby increasing the contact lengths between adjacent layers. Furthermore, in all cases, the contact lengths increase under pressure, while the void lengths decrease under pressure. This results in increased contact areas across the interfaces in the OPV structures. Hence, the higher power conversion efficiency of ~25% observed after the application of pressure is attributed largely to the increased contact areas due to the application of pressure.

Hence, the performance of OPV structures can be enhanced by the application of controlled levels of pressure during lamination and stamping processes. Such pressure may be applied after using the conventional spin-coating and thermal evaporation techniques to deposit the individual layers in the OPV structures. However, care is needed to ensure that the applied pressure does not exceed ~ 10 MPa in P3HT:PCBM systems due to the potential for excessive layer deformation and/or particle sink-in, which may cause damage to the device.

The required balance of improved contact without excessive sink-in can also be guided using the results of the analytical and computational models presented in this paper. Such developments could facilitate the development of fast, low-cost stamping and roll-to-roll processes,[27] for the fabrication of efficient OPV structures.

V. Summary and Concluding Remarks

This paper presents the results of a combined analytical, computational and experimental study of interfacial surface contacts and the performance of OPVs. The models predict the interfacial surface contacts increase with increasing adhesion energies (between adjacent surface layers) and adhesion layers. However, excessive pressure application can lead to device

degradation and damage. The predictions from the models were also verified with experiments that show that pressures up to ~ 10 MPa result in improved power conversion efficiencies from ~3.5% to ~4.4%.

Acknowledgements

We appreciate the World Bank African Centers of Excellence program, the World Bank STEP-B, the Nelson Mandela Institution and the Rutgers University for the supporting this research. B. Agyei-Tuffour also appreciates the Carnegie Corporation New York for the sponsorship through the Next Generation of African Academics program at the University of Ghana. Professor Manish Chowolla and Prof. Eric Garfunkel are specially acknowledged for their useful technical discussions and assistance. Brookhaven National Laboratory and Dr. Kevin Yager are acknowledged for the help with the synchrotron analysis.

References

1. S. B. Darling, F. You, T. D. Veselka, A. Velosa, *Ener. & Envir. Sci.,* **4,** 3133–3139, (2011).
2. S. A. Choulis, A. Patwardhan, M. K. Mathai, V. -E. Choong and F. So, *Adv. Funct. Mater.,* **16 (8)**, 1075–1080, (2006).
3. T. M. Brown, J. S. Kim, R. H. Friend, F. Cacialli, R. Daik and W. J. Feast, *Appl. Phys. Lett.,* **75** (12), 1679–1681, (1999).
4. V. Shrotriya, G. Li, Y. Yao, C-W. Chu and Y. Yang, *Appl. Phys. Lett.,* **88**, 073508, (2006).
5. J. Du, V. C. Anye, E. O. Vodah, T. Tong, M. G. Zebaze Kana and W. O. Soboyejo, *J. Appl. Phys.,* **115**, 233703, (2014).
6. T. Tong, B. Babatope, S. Admassie, J. Meng, O. Akwogu, W. Akande and W. O. Soboyejo, *J. Appl. Phys.,* **106**, 083708, (2009).
7. B. Agyei-Tuffour, E.R. Rwenyagila, J. Asare, O.K. Oyewole, M.G. Zebaze Kana, D.M. O'Carroll, W.O. Soboyejo, *Adv. Mater. Res*. Vol. **1132,** 204-216, (2016).
8. K. J. Reynolds, J. A. Barker, N. C. Greenham, R. H. Friend, and G. L. Frey, J. Appl. Phys. 92, 7556 (2002).
9. H. You, Y. Dai, Z. Zhang, and D. Ma, J. Appl. Phys. 101, 026105 (2007).
10. W.-J. Shin, J.-Y. Lee, J. C. Kim, T.-H. Yoon, T.-S. Kim, and O.-K. Song, Org. Electron. 9, 333–338 (2008).
11. C. J. Brabec, V. Dyakonov, J. Parisi, N.S. Sariciftci (Eds.), *Springer-Verlag,* Heidelberg, (2003).
12. G. Yu, J. Gao, J. C. Hummelen, F. Wudl, A. J. Heeger, *Science,* **270,** 1789, (1995).
13. S. E. Shaheen, C. J. Brabec, N. S. Sariciftci, F. Padinger, T. Fromherz, J. C. Hummelen, *Appl. Phys. Lett.,* **78,** 841, (2001).
14. C.J. Brabec, J.C. Hummelen, N.S. Sariciftci, *Adv. Mater.,* **11**. (2001).

15. S. Sapp, S. Luebben, Y. B. Losovyj, P. Jeppson, D. L. Schulz, and A. N. Caruso, *Appl. Phys. Lett.,* **88**, 152107, (2006).

16. L. Fengmin, S. Shuyan, G. Xiaoyang, Z. Yun and X. Zhiyuan, *Sol. Energ. Mater. & Sol. Cells*, **94**, 842–845, (2010).

17. W. M. Moreau: Semiconductor Lithography: Principles, Practices and Materials (*Plenum Press,* New York, 1988).

18. Y. Cao, C. Kim, S. R. Forrest, and W. Soboyejo, *J. Appl. Phys.,* **98**, 033713, (2005).

19. D. Maugis, M. Barquins and R. Courtel, *Metaux-Corrosion-Industrie*, **605,** 1-10, (1976).

20. International Organization for Standardization, ISO 14644-1:1999, Clean Rooms and Associated Controlled Environments-Part I: Classification of Air Cleanliness (ISO, Switzerland, (1999)).

21. B. M. Malyshev and R. L. Salganik, *Int. J. Fract*., **26**, 261–275, (1984).

22. K. Wan and Y. Mai, *Int. J. Fract*. **74**, 181–197, (1995).

23. T. M. Tong, PhD Thesis (Princeton University, 2012).

24. W. O. Akande, Y. Cao, N. Yao and W. Soboyejo. *J. Appl. Phys.,* **107**, 043519, (2010).

25. B. V. Derjaguin and V. M. Muller and Y. P. Toporov, *J. Col. Inter. Sci.* **53**, 314–325. (1975).

26. J. A. Greenwood, *Proc. R. Soc. Lond.* A **453**, 1277-1297, (1997).

27. S. R. Forrest, *Nature,* **428**, 911–918, (2004).

28. J. Asare, S. A. Adeniji, O. K. Oyewole, B. Agyei-Tuffour, J. Du, E. Arthur, A. A. Fashina, M. G. Zebaze Kana and W. O. Soboyejo, AIP Adv., **6**, 065125, and (2016).

29. B. Agyei-Tuffour, E.R. Rwenyagila, J. Asare, M.G. Zebaze Kana, W.O. Soboyejo, *J. Mater. Res*., (2016). DOI: 10.1557/jmr.2016.344

30. W. D. Callister: Materials Science and Engineering: An Introduction (*Wiley, New York*, 2003)

31. Y. Guo, X. J. Ma and Z. H. Su, *Macromolecules*, **46**, 2733–2739 (2013).

32. F-Ching Tang, J. Chang, F.-C. Wu, H.-L. Cheng, S. L.-C. Hsu, J.-S. Chen and W.-Y. Chou, *J. Mater. Chem.*, (2012) DOI: 10.1039/c2jm34556k

33. W. Zhou, J. Shi, L. Lv, L. Chen and Y. Chen, *Phys. Chem. Chem. Phys.*, **17**, 387-397, (2015).

34. A. Ashraf, D. M. N. M. Dissanayake and M. D. Eisaman, *Phys. Chem. Chem. Phys (*2015), DOI: 10.1039/c5cp03399c

35. Z. Shen and D.M. O'Carroll: Adv. Funct. Mater. **25**, 3302–3313 (2015).

List of Tables

Table I

Particles	Surface roughness (nm)	Young's modulus (GPa)	Adhesion Energy (J/m^2)
	Rigid particles		
Aluminum	2.4 ± 0.4	70	12
ITO	2.9 ± 0.5	116	9.3
MoO_3	0.7 ± 0.3	64.6	6.2
Glass	1 ± 0.3	70	9.3
	Semi-rigid particles		
MEH-PPV (OLEDs)	2.2 ± 0.7	11.5	0.8
P3HT:PCBM (OPVs)	0.7 ± 0.3	6.02	2.9
	Compliant particles		
PEDOT:PSS	0.8 ± 0.1	1.56	0.5

Table II

OPV Device	Open Circuit Voltage, V_{oc} (V)	Short Circuit Current, I_{sc} (mA/cm^2)	Power Conversion Efficiency PCE (%)
OPV_0	0.62	10.73	3.5
OPV_{10}	0.60	13.10	4.4

List of Figures

Figure 1 Bilayered and multilayered nanostructures adopted in the pressure assisted organic photovoltaic cell fabrication: (a) rough surface contacts with blister height, (b) smooth surface contact with trapped particle and (c) complete device showing multilayers with pressure application.

Figure 2 The surface/interface morphology of the OPV layered structures acquired from the SEM before and after the application of pressure. The images in Fig. 2(a) – 2(f) show the rough surfaces increasingly smoothening with pressure to enhance interfacial contacts between the films. Figures: (a) 1 MPa, (b) 3 MPa, (c) 5 MPa, (d) 8 MPa, (e) 10 MPa and (f) 15 MPa. The inserts 2(i-vi) are the optical micrographs of the polymer blends with different applied pressures as above.

Figure 3 Polymer crystallinity and chain alignments upon pressure application: (a) GIWAXS representation of the polymer blend-substrate-x-ray interactions, (b) 1D out-of-plane peaks: (100), (200), (300) and in-plane profile showing the (010) dominant peak of P3HT films and (c) the out of plane peak directions ((100), (200) and (300)) indicating the orientation of P3HT crystallites in P3HT:PCBM blends.[21,29,31-35]

Figure 4 shows the ultra-violet-visible (UV-Vis) enhancements in the photo-absorbance of P3HT:PCBM thin films upon the application of pressure.[7,29] The pressure applied include: pressure-less, 1 MPa, 3 MPa, 5 MPa, 8 MPa, 10 MPa and 15 MPa.

Figure 5 Analytical modeling of the interfacial surface contacts and their dependence on (a) pressure and (b) adhesion energy between the OPV layers.

Figure 6 Finite element model of surface contact during OPV layer deposition with a trapped particle between any two layers. The geometry and mesh show the formation of blisters and the evolution of contact during pressure application on the PDMS stamp.[5,28]

Figure 7 Stress distributions induced by trapped particles and OPV layers: (a) von Mises stress distribution in and around the trapped particle and in the films, (b) the sink-in phenomena of OPV layers and trapped particles and the associated stress distributions in the layered structures.

Figure 8 Schematic diagram of the deformation profiles of trapped particle between PEDOT.PSS film and glass substrate with the application of pressure. The height of the particles: rigid, semi-rigid and compliant are h_r, h_{sr} and h_c, respectively.[28]

Figure 9 Power conversion efficiency and current-voltage characteristics of organic photovoltaic devices under pressure application.

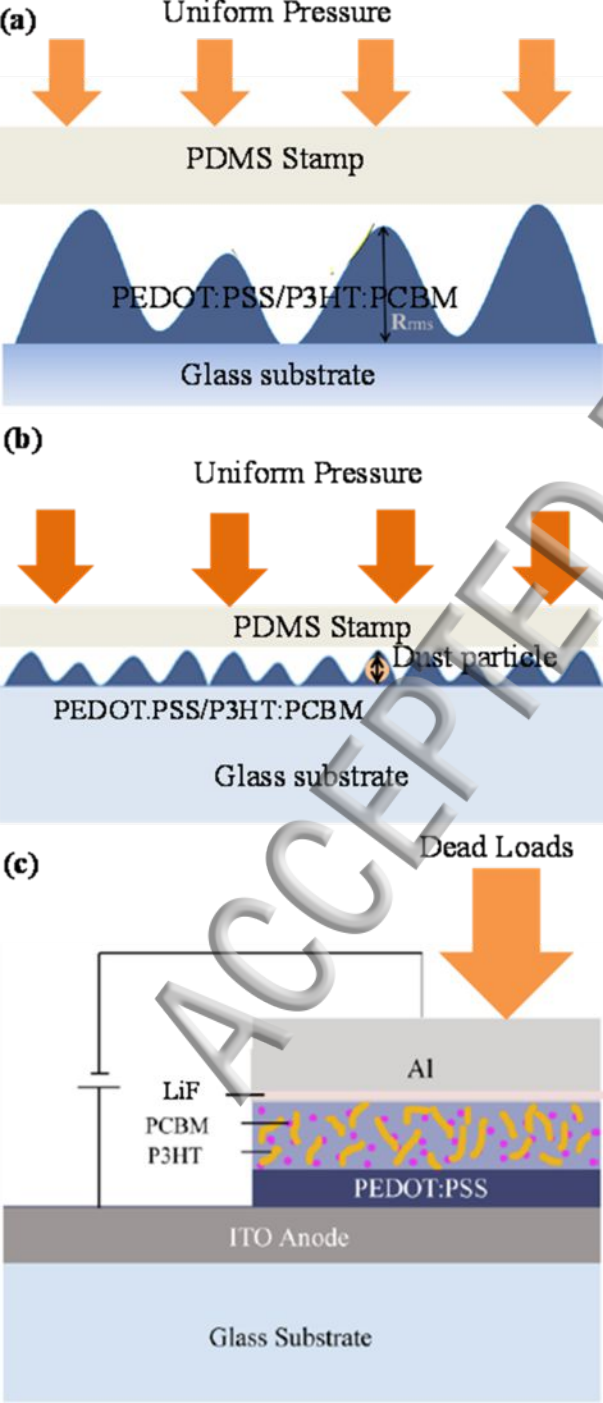
(a)
Uniform Pressure
PDMS Stamp
PEDOT:PSS/P3HT:PCBM
Rms
Glass substrate
(b)
Uniform Pressure
PDMS Stamp
Dust particle
PEDOT:PSS/P3HT:PCBM
Glass substrate
(c)
Dead Loads
Al
LiF
PCBM
P3HT
PEDOT:PSS
ITO Anode
Glass Substrate

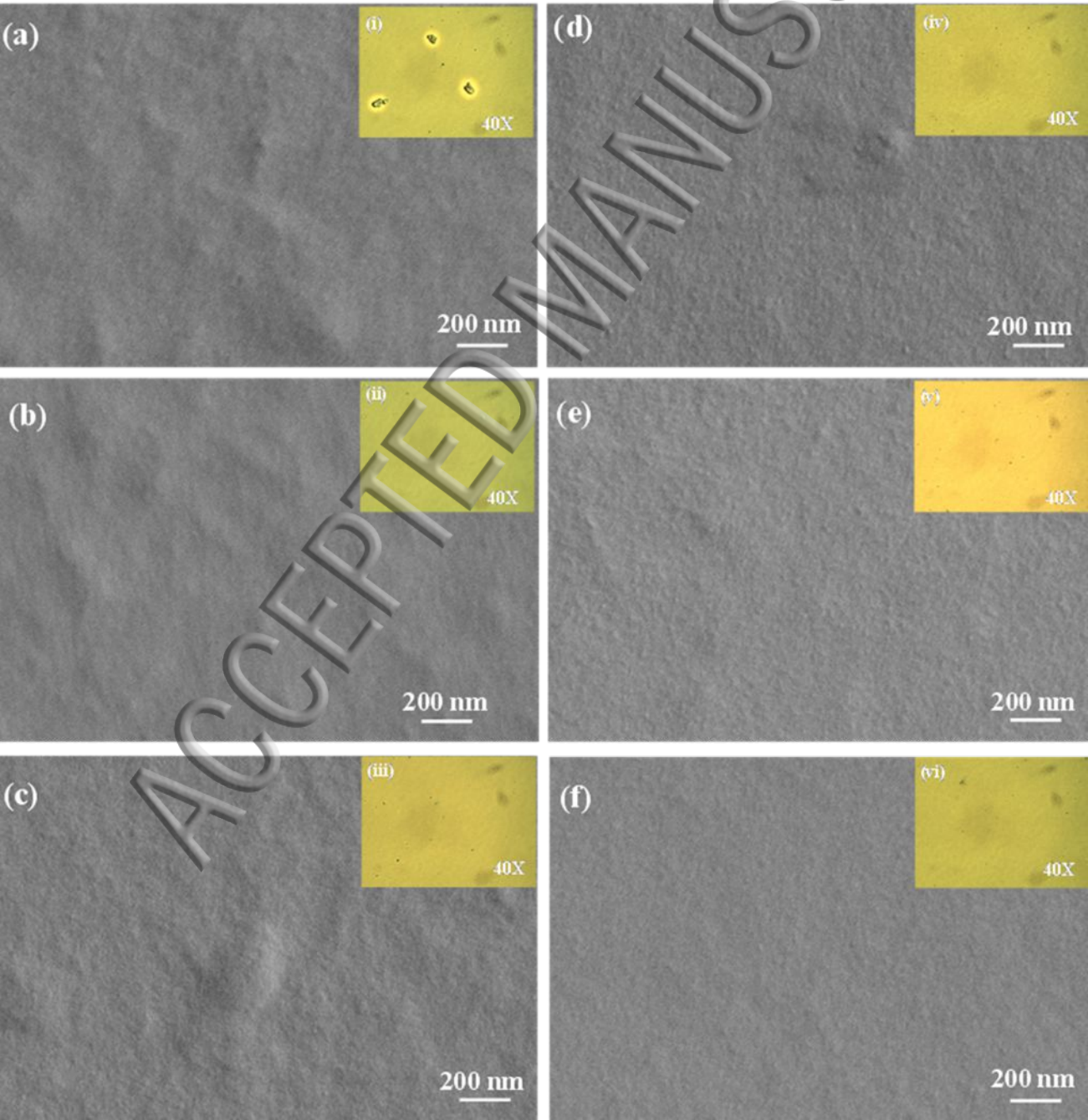

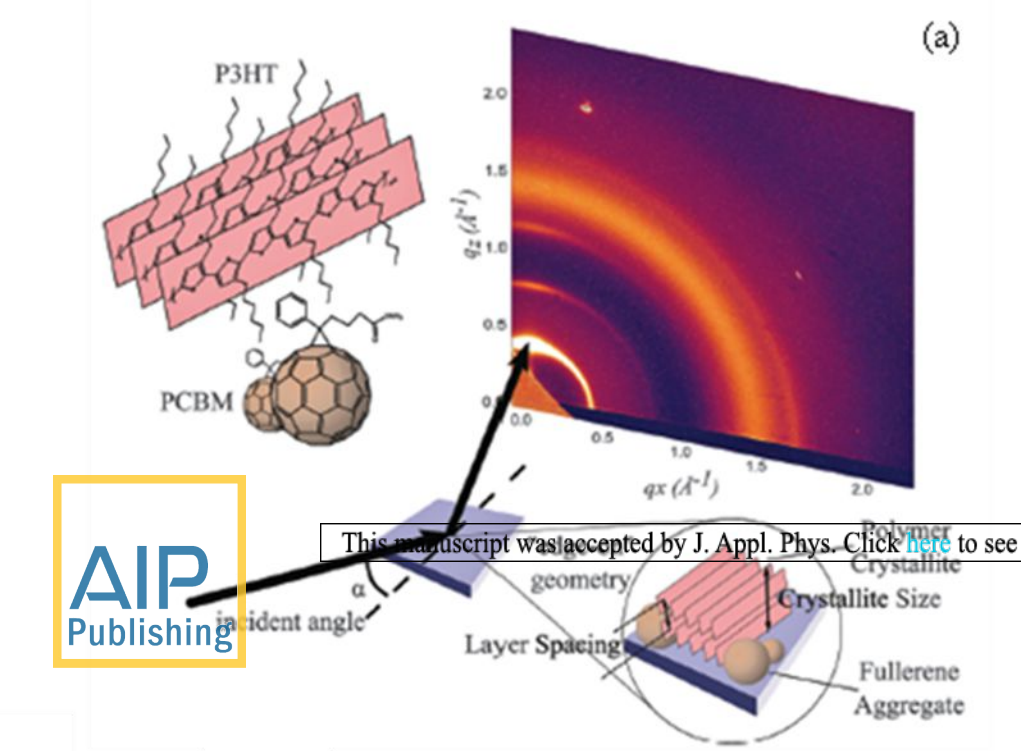

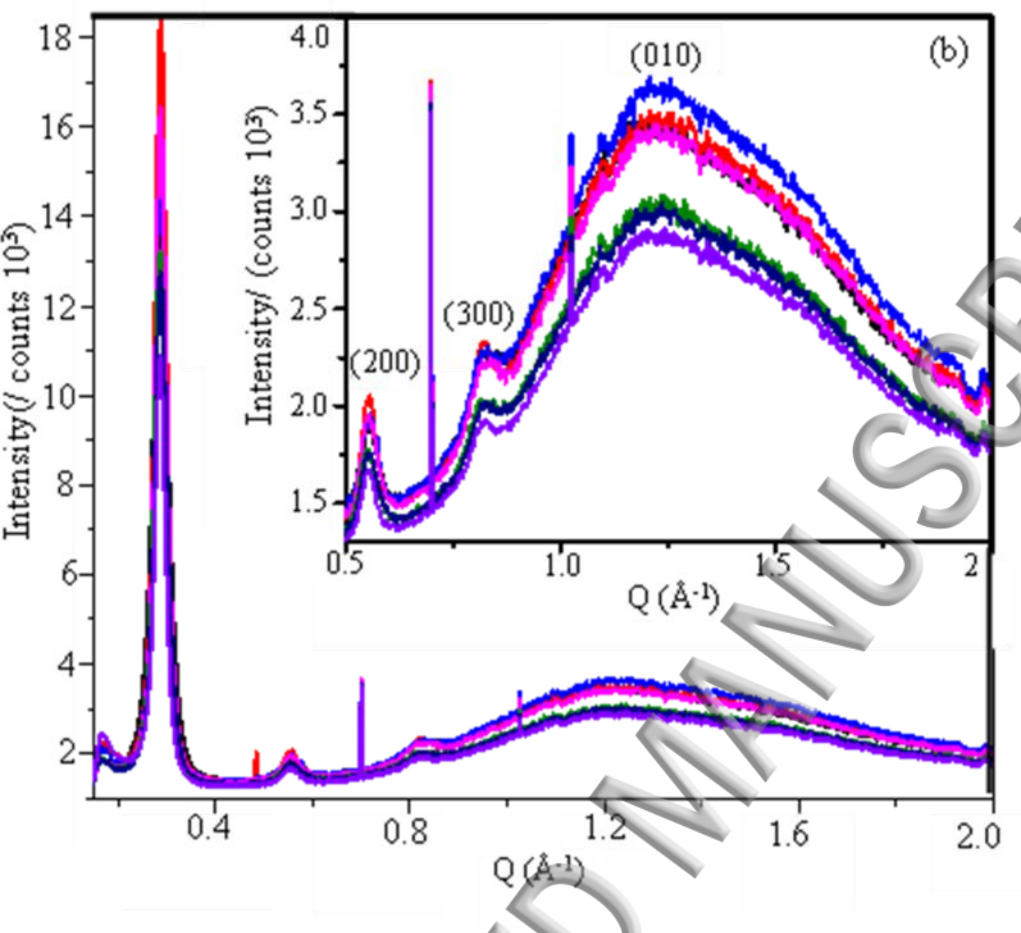

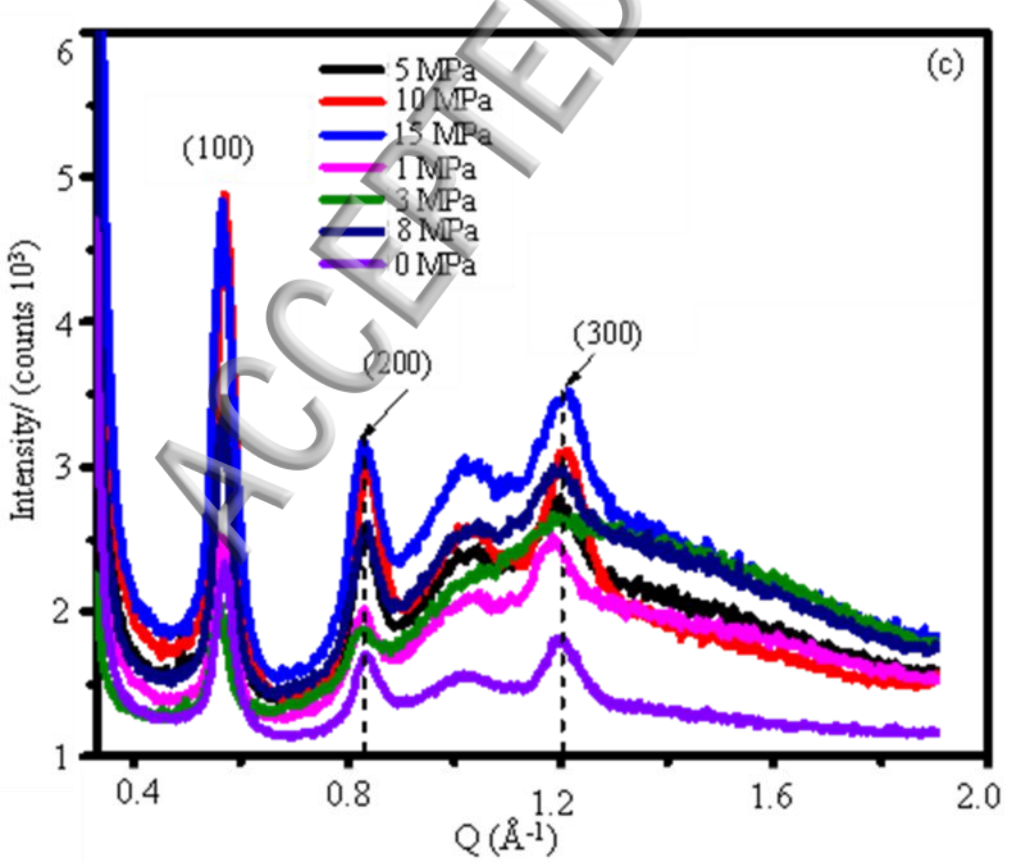

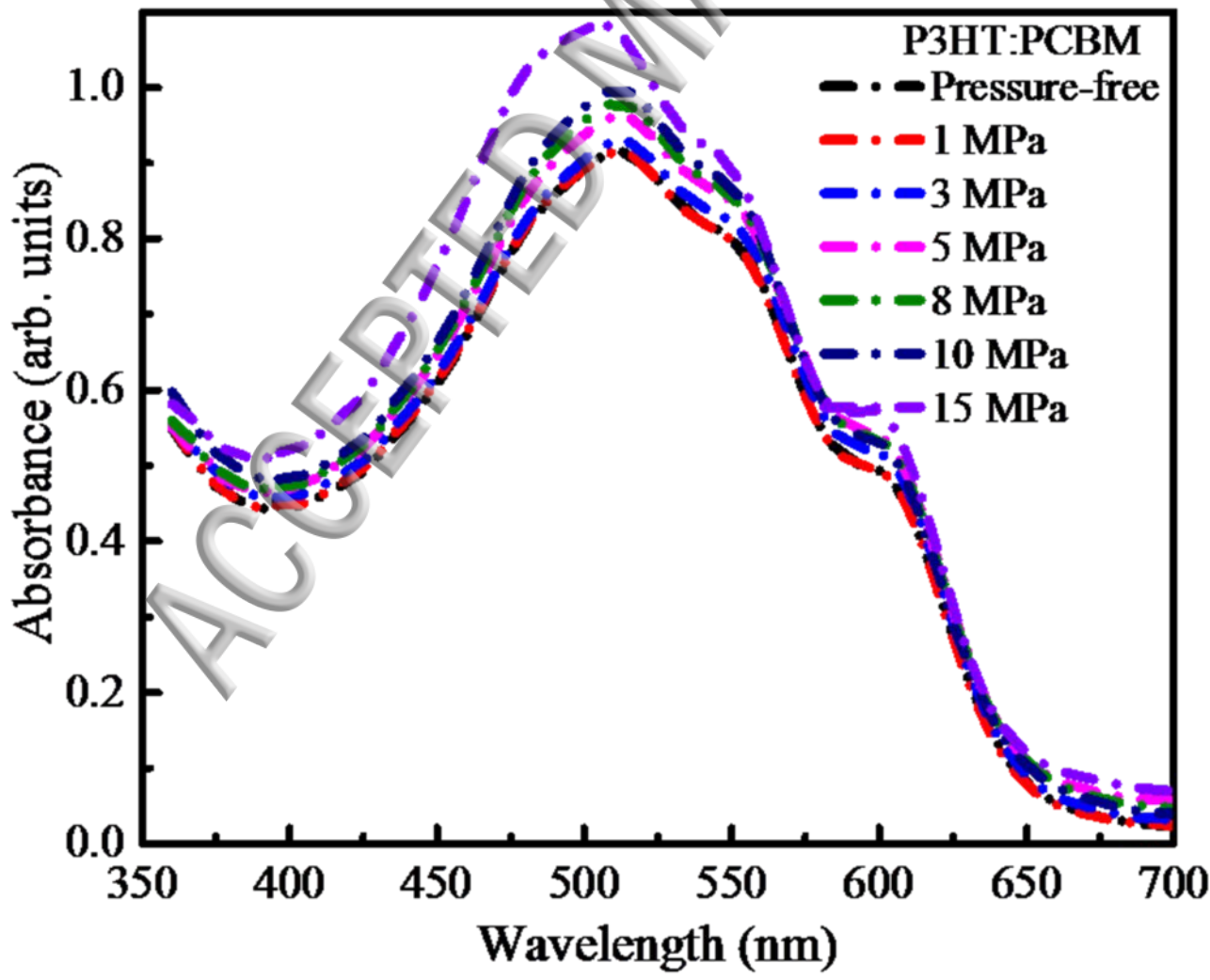
P3HT:PCBM
Pressure-free
1 MPa
3 MPa
5 MPa
8 MPa
10 MPa
15 MPa
Absorbance (arb. units)
Wavelength (nm)
0.0
0.2
0.4
0.6
0.8
1.0
350
400
450
500
550
600
650
700

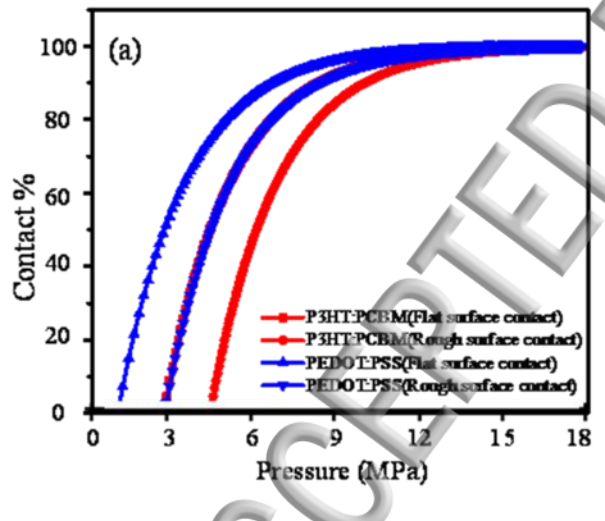
(a)
Contact %
Pressure (MPa)
P3HT:PCBM(Flat surface contact)
P3HT:PCBM(Rough surface contact)
PEDOT:PSS(Flat surface contact)
PEDOT:PSS(Rough surface contact)

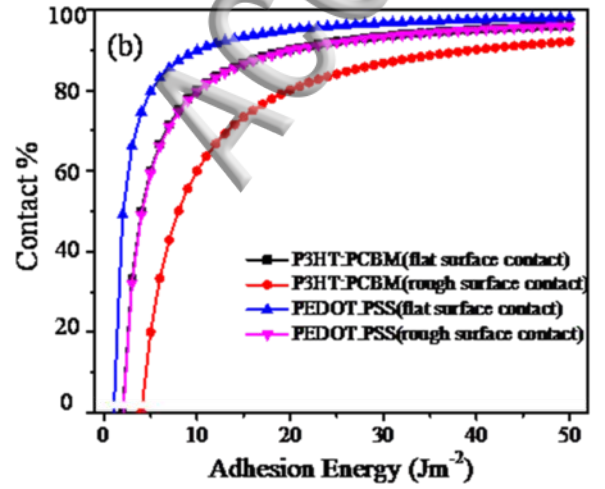
(b)
Contact %
Adhesion Energy (Jm-2)
P3HT:PCBM(flat surface contact)
P3HT:PCBM(rough surface contact)
PEDOT:PSS(flat surface contact)
PEDOT:PSS(rough surface contact)

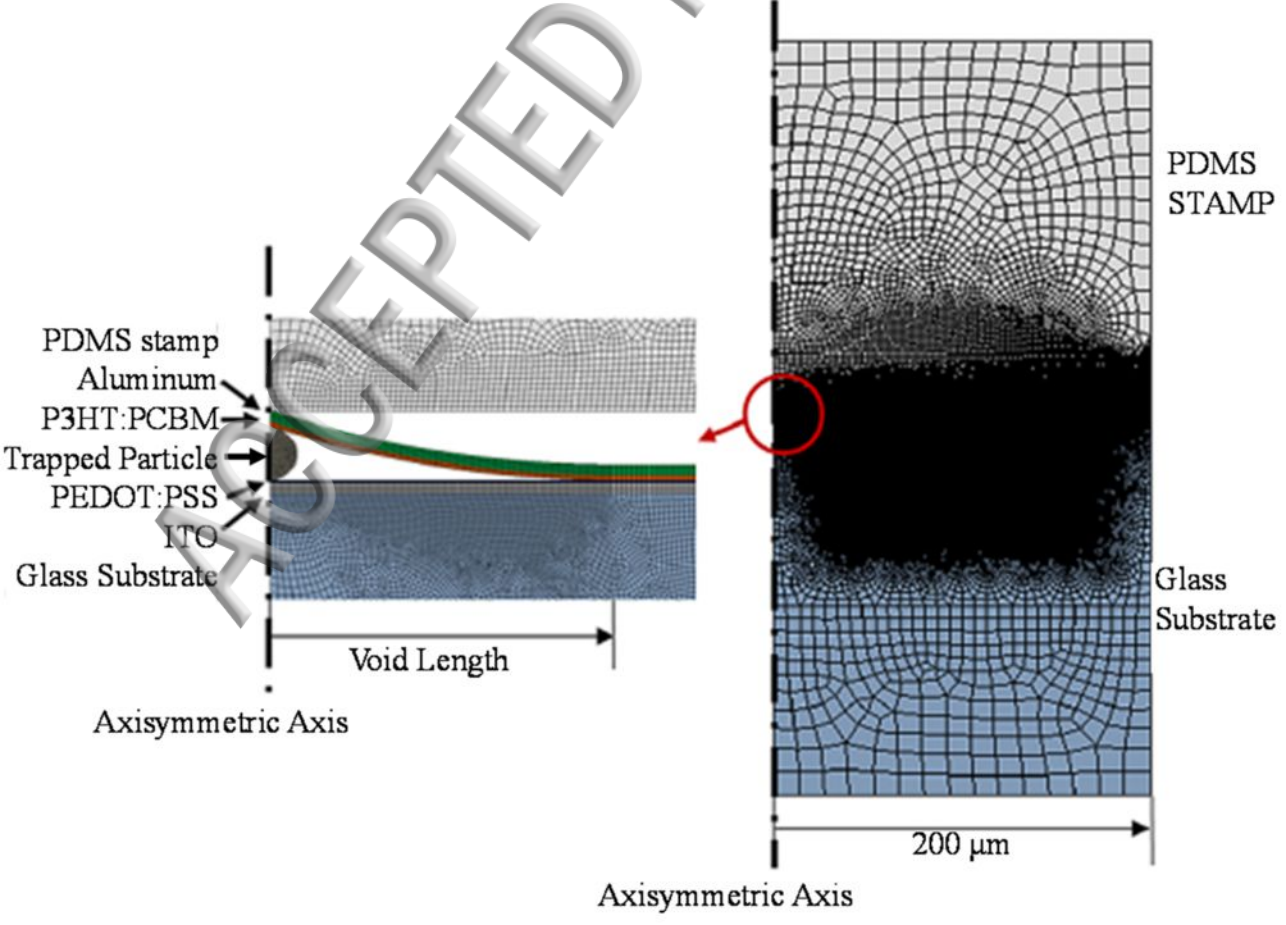
PDMS stamp
Aluminum
P3HT:PCBM
Trapped Particle
PEDOT:PSS
ITO
Glass Substrate
Void Length
Axisymmetric Axis
PDMS
STAMP
Glass
Substrate
200 μm
Axisymmetric Axis

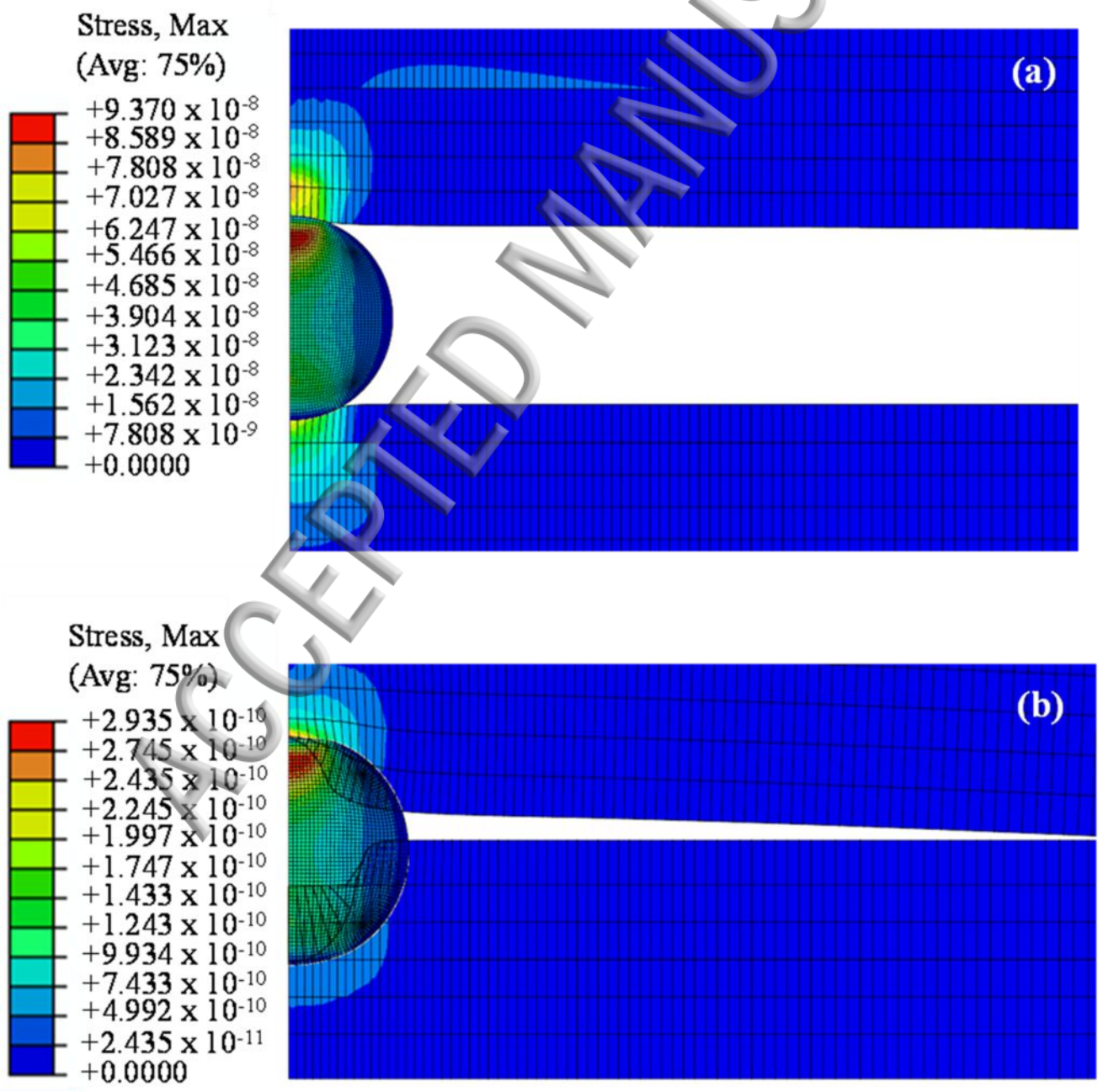

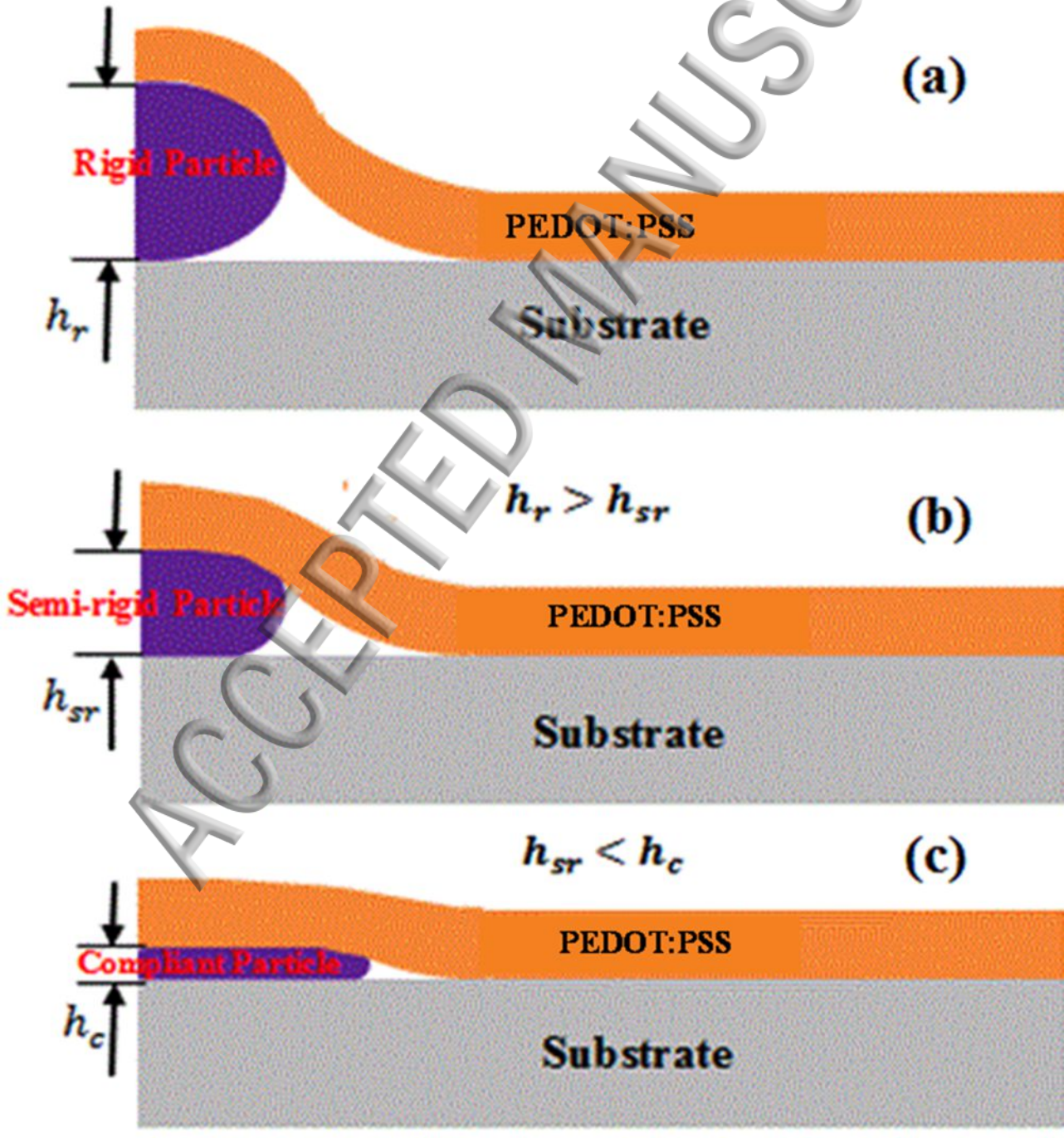

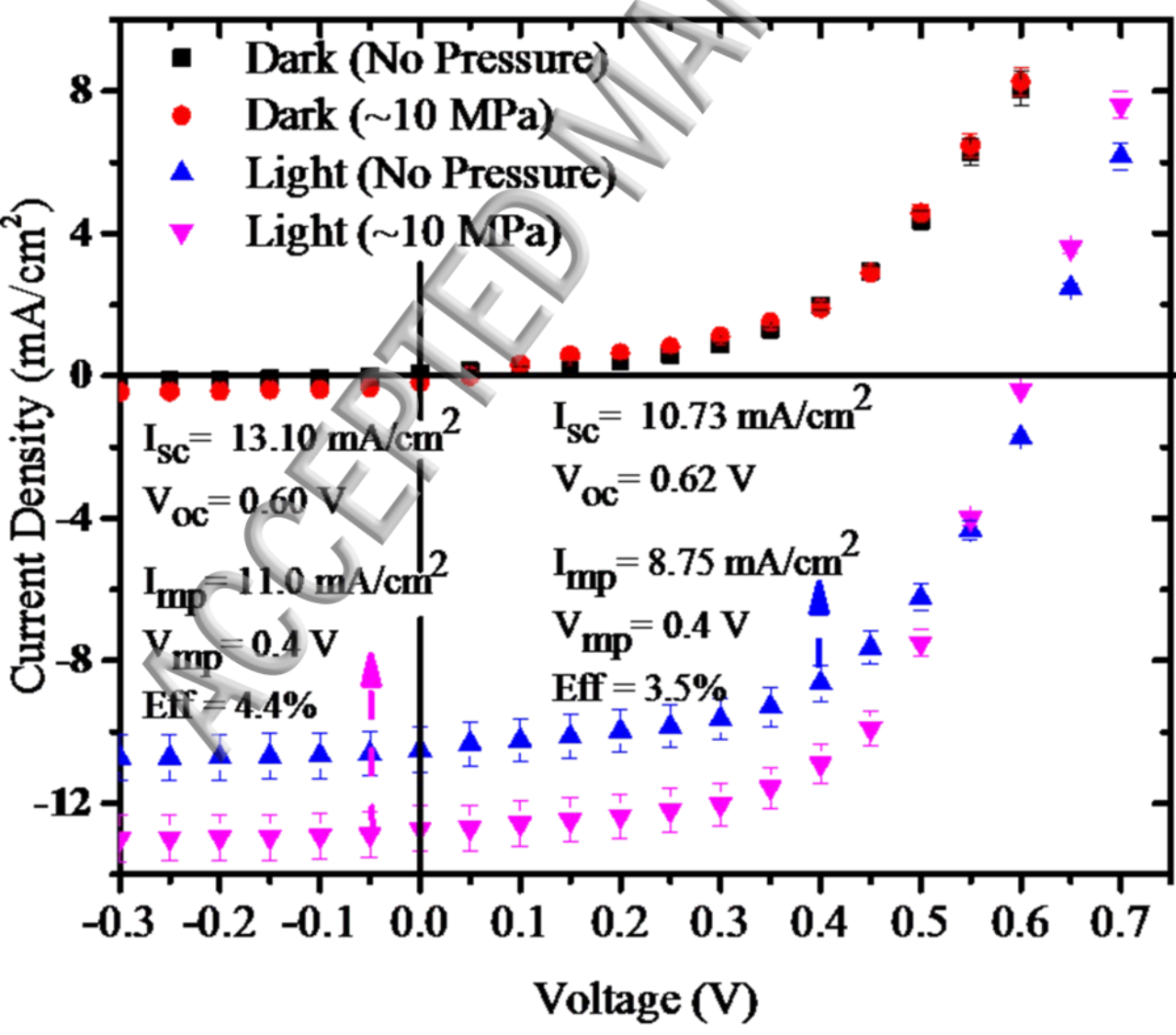
Dark (No Pressure)
Dark (~10 MPa)
Light (No Pressure)
Light (~10 MPa)
I_{sc}= 13.10 mA/cm^2
V_{oc}= 0.60 V
I_{mp}= 11.0 mA/cm^2
V_{mp}= 0.4 V
Eff = 4.4%
I_{sc}= 10.73 mA/cm^2
V_{oc}= 0.62 V
I_{mp}= 8.75 mA/cm^2
V_{mp}= 0.4 V
Eff = 3.5%
Current Density (mA/cm^2)
Voltage (V)
8
4
0
-4
-8
-12
-0.3
-0.2
-0.1
0.0
0.1
0.2
0.3
0.4
0.5
0.6
0.7